Published in final edited form as:
Bioconjug Chem. 2012 January 18; 23(1): 115–124. doi:10.1021/bc200546b.

Synthesis and Evaluation of Novel Tc-99m Labeled Probestin Conjugates for Imaging APN/CD13 Expression In Vivo

Gopal Pathuri[†], **Andria F. Hedrick**[†], **Bryan Disch**[†], **John Doan**[§], **Michael A. Ihnat**[†,‡], **Vibhudutta Awasthi**[†], and **Hariprasad Gali**[†,‡,*]

[†]Department of Pharmaceutical Sciences, College of Pharmacy, The University of Oklahoma Health Sciences Center, Oklahoma City, OK 73117, USA

[§]Department of Radiological Sciences, Division of Nuclear Medicine, College of Medicine, The University of Oklahoma Health Sciences Center, Oklahoma City, OK 73117, USA

[‡]Experimental Therapeutics Program, Peggy and Charles Stephenson Oklahoma Cancer Center, The University of Oklahoma Health Sciences Center, Oklahoma City, OK 73117, USA

Abstract

The enzyme aminopeptidase N (APN, also known as CD13) is known to play an important role in tumor proliferation, attachment, angiogenesis, and tumor invasion. In this study, we hypothesized that a radiolabeled high affinity APN inhibitor could be potentially useful for imaging APN expression in vivo. Here we report synthesis, radiolabeling, and biological evaluation of new probestin conjugates containing a tripeptide, *N*,*N*-dimethylglycyl-L-lysinyl-L-cysteinylamide (N_3S), chelator. New probestin conjugates were synthesized by solid-phase peptide synthesis method, purified by reversed-phase HPLC, and characterized by electrospray mass spectrometry. The conjugates were complexed with Re(V) and ^{99m}Tc(V) by transmetallation using corresponding Re(V) or ^{99m}Tc(V) gluconate synthon. The mass spectral analyses of ReO-N_3S-Probestin conjugates were consistent with the formation of neutral Re(V)O-N_3S complexes. Initial biological activity of ReO-N_3S-Probestin conjugates determined by performing an *in vitro* APN enzyme assay using intact HT-1080 cells demonstrated higher inhibition of APN enzyme activity than bestatin. *In vivo* biodistribution and whole body planar imaging studies of ^{99m}TcO-N_3S-PEG_2-Probestin performed in nude mice xenografted with human fibrosarcoma tumors derived from HT-1080 cells demonstrated a tumor uptake value of 2.88 ± 0.64 %ID/g with tumor-to-blood and tumor-to-muscle ratios of 4.8 and 5.3 respectively at 1 hr post-injection (p.i.). Tumors were clearly visible in whole-body planar image obtained at 1 hr p.i., but not when the APN was competitively blocked with a co-injection of excess non-radioactive ReO-N_3S-PEG_2-Probestin conjugate. These results demonstrate the feasibility of using high affinity APN inhibitor conjugates as targeting vectors for *in vivo* targeting of APN.

Keywords

Aminopeptidase N; APN; CD13; probestin; bestatin; tumor angiogenesis; Tc-99m; N3S chelator; SPECT; imaging

[*]Correspondence to: Hariprasad Gali, The University of Oklahoma College of Pharmacy, 1110 N. Stonewall Avenue, Room 301, Oklahoma City, OK 73117, USA, hgali@ouhsc.edu, Phone: (405) 271-6593 Ext 47877, FAX: (405) 271-7505.

Introduction

Aminopeptidase N (APN, EC 3.4.11.2) is a zinc-dependent membrane-bound exopeptidase that catalyzes the removal of N-terminal amino acids from peptides.[1, 2] It is expressed by many tissues, particularly the brush border membrane of the small intestine, the proximal renal tubules, synaptic membranes in the central nervous system, and monocytes and granulocytes.[1–5] Look et al. reported that human myeloid plasma membrane glycoprotein CD13 is identical to APN.[1] High levels of APN/CD13 expression have been detected in various solid tumors.[4, 6–10] APN/CD13 is shown to play an active role in degradation and invasion of extracellular matrix by metastatic tumor cells.[11, 12] Pasqualini et al. have shown that APN/CD13 is specifically expressed on the endothelium of tumor angiogenic, but not normal, vasculature.[13] APN inhibitors, such as inhibitory antibodies and bestatin (ubenimex), suppressed angiogenesis and tumor growth.[13] Bhagwat et al. have shown that endogenous APN/CD13 levels in primary cells and cell lines are up-regulated in response to hypoxia, angiogenic growth factors, and signals regulating capillary tube formation during angiogenesis.[14] APN inhibitors interfered with tube formation but not proliferation of primary vascular endothelial cells, suggesting that APN/CD13 functions in the control of endothelial cell morphogenesis.[14] The association of APN/CD13 with the growth of different human cancers suggested it as a suitable target for anticancer therapy. Thus, several new diagnostic and therapeutic constructs directed towards APN/CD13 have been developed.[13, 15–27] These constructs utilized a cyclic CNGRC peptide known to bind APN/CD13.[13]

Recent studies have shown that asparagine-glycine-arginine (NGR) motif can rapidly convert to isoaspartate-glycine-arginine (*iso*DGR) by asparagine deamidation, generating $\alpha_v\beta_3$ ligands capable of affecting endothelial cell functions and tumor growth.[28–32] Biochemical, NMR structure analysis, and $\alpha_v\beta_3$ docking studies showed that *iso*DGR, but not NGR and DGR, can fit into the RGD-binding pocket of $\alpha_v\beta_3$ integrin, recapitulating not only the canonical RGD/$\alpha_v\beta_3$ contacts but also establishing additional polar interactions.[28, 30] However, it is unclear whether cyclic CNGRC peptide based constructs reported so far were binding APN/CD13 or $\alpha_v\beta_3$ integrin under tested in vivo conditions. Our recent in vivo blocking studies using a ^{99m}Tc-labeled cyclic C*iso*DGRC conjugate demonstrated a selective binding to the tumors and other tissues expressing $\alpha_v\beta_3$-integrin.[33] Furthermore, cyclic CNGRC peptide is shown to have moderate binding affinity to APN as evidenced by enzyme inhibition studies.[34]

We hypothesized that a radiolabeled high affinity APN inhibitor could be potentially useful for imaging APN expression in vivo. We designed and evaluated two novel probestin conjugates to examine our hypothesis. Probestin is a high affinity inhibitor of APN.[35] Here we report synthesis, radiolabeling, and biological evaluation of the new probestin conjugates containing a tripeptide, *N*,*N*-dimethylglycyl-L-lysinyl-L-cysteinylamide (N_3S), chelator.

Materials and Methods

General

All chemicals obtained commercially were used without further purification. Bestatin was obtained from Acros Organics (Geel, Belgium). Fmoc-bestatin was synthesized as previously reported.[36] Rink amide MBHA resin (100–200 mesh, 0.3–0.8 mmol/gm) and Fmoc-LYS(ivDde)-OH were obtained from EMD Chemicals Inc. (Gibbstown, NJ). Fmoc-8-amino-3,6-dioxaoctanoic acid (PEG_2) was obtained from Peptides International Inc. (Louisville, KY). Fmoc-DAP(ivDde)-OH was obtained from Bachem Americas, Inc. (Torrance, CA). Other Fmoc-protected amino acids and coupling agents were obtained from Advanced ChemTech (Louisville, KY). Chemicals used for peptide cleavage were obtained

from Sigma-Aldrich (St. Louis, MO). BDH® brand ACS grade solvents were obtained from VWR International, LLC (Radnor, PA). $Na^{99m}TcO_4$ was obtained from the University of Oklahoma Nuclear Pharmacy. Human fibrosarcoma HT-1080 cells were obtained from American Type Culture Collection (Manassas, VA). The cells were cultured in ATCC-formulated Eagle's Minimum Essential Medium supplemented with 10% fetal calf serum (Invitrogen Corporation, Carlsbad, CA) and 1% Pen Strep (Invitrogen Corporation, Carlsbad, CA) containing 10,000 units of penicillin and 10,000 μg of streptomycin per ml. Cells were grown routinely in a monolayer culture at 37°C in a 5% CO_2 humidified air atmosphere. Eight-week old female athymic nude NU/J mice (Homozygous for *Foxn1*^{nu}) were purchased from the Jackson Laboratory (Bar Harbor, ME). Electrospray mass spectral analysis was performed by the University of Oklahoma Health Sciences Center (OUHSC) Molecular Biology-Proteomics Facility. The small animal SPECT imaging was conducted in the OU College of Pharmacy Research Imaging Facility using a two-detector NanoSPECT In Vivo Preclinical Imager (Bioscan, Inc., Washington, DC, USA). All animal studies were conducted in accordance with the protocols approved by the OUHSC institutional animal care and use committee.

Reversed-phase HPLC analyses of N_3S-Probestin conjugates and their Re(V)/^{99m}Tc(V) complexes were performed on a Beckman System Gold HPLC equipped with a Beckman Model 126 pump, 166 absorption detector, and a Bioscan Model B-FC-300 radioactivity detector. HPLC solvents consisted of water containing 0.1% trifluoroacetic acid (solvent A) and acetonitrile containing 0.1% trifluoroacetic acid (solvent B). A Sonoma C_{18} (ES Industries, 10 μm, 100 Å, 4.6 × 250 mm) column was used with a flow rate of 1.5 mL/min. The HPLC gradient system began with an initial solvent composition of 95% A and 5% B for 2 minutes followed by a linear gradient to 50% A and 50% B in 15 minutes, after which the column was reequilibrated. The absorption detector was set at 254 nm.

Solid phase peptide synthesis (SPPS)

SPPS was performed manually using conventional Fmoc chemistry. Standard side chain protecting groups were utilized and the peptide was assembled on Rink amide resin (0.05 mmol) using HBTU-mediated coupling as shown in Figure 1. Amino acid coupling was achieved by treating the resin with Fmoc-protected amino acid (3.3 eq) in DMF (500 μl), HBTU (3.3 eq) in DMF (500 μl), HOBt (3.3 eq) in DMF (250 μl), and DIPEA (6.6 eq) in DMF (250 μl) for 60 min at room temperature followed by five washes with DMF (1 ml). The Fmoc deprotection was achieved by treating the resin with 20% piperidine in DMF (2 ml) for 1 × 10 min and 1 × 20 min at room temperature followed by five washes with DMF (1 ml). Orthogonally-protected Lys, Fmoc-Lys(ivDde)-OH or Fmoc-DAP(ivDde)-OH was used to obtain the tripeptide chelator sequence (DMG-Lys-Cys orDMG-DAP-Cys). The ivDde group was selectively deprotected by treating the resin with 2% hydrazine in DMF (2 ml) for 1 × 10 min and 1 × 20 min at room temperature followed by five washes with DMF (1 ml). Finally, the resin was washed five times with DMF (1 ml) followed by dichloromethane (1 ml), and dried for 30 min by nitrogen purging. The peptide was cleaved from the resin and the side chains were deprotected by treating the resin with a cocktail (1 ml) containing trifluoroacetic acid, water, ethanedithiol, and thioanisol in a ratio of 90:2.5:2.5:5 for 2 hr at room temperature. The crude peptide was isolated by precipitation in ice cold methyl-*t*-butyl ether, purified by HPLC, and dried on a rotary evaporator under vacuum. After drying, the peptide was dissolved in 0.1 M ascorbic acid (2 mg/ml) and aliquots of 50 μl were dispensed into 1.5 ml microcentrifuge tubes and dried using SpeedVac centrifugation. The tubes containing N_3S-Probestin conjugate (~100 μg) and ascorbic acid (~880 μg) were stored at −20 °C and used for radiolabeling with Tc-99m. The N_3S-Probestin conjugates were characterized by electrospray mass spectrometry.

Re(V) complexation

Re complexation of N_3S-Probestin conjugates was achieved by transmetallation from Re(V)-gluconate prepared as previously described.[37] Briefly, a stock solution of Re(V)-gluconate was freshly prepared by mixing a nitrogen-purged (5 min) solution of $SnCl_2$ (32 mg) in 0.1 M HCl (200 µl) with a nitrogen-purged (10 min) solution of ammonium perrhenate (45.5 mg) in 0.5 M sodium gluconate (2.5 ml) and incubated at RT for over 1 hr until the solution is turned to deep blue color. For complexation, an aliquot of Re(V)-gluconate stock solution (100 µl) and 0.5 M sodium gluconate (400 µl) were added to N_3S-Probestin conjugate (5 mg), vortexed for 30 sec, and incubated at RT for 1 hr. The ReO-N_3S-Probestin conjugate was then purified by HPLC and analyzed by electrospray mass spectrometry. The ReO-N_3S-Probestin conjugates were obtained in >85% yield after HPLC purification.

Tc-99m labeling

The N_3S-Probestin was labeled with ^{99m}Tc by transmetallation from ^{99m}Tc(V)-gluconate.[38] Briefly, a stannous gluconate stock solution was prepared by mixing $SnCl_2$ (2 mg) in nitrogen-purged (10 min) 0.5 M sodium gluconate (1 ml). A diluted stock solution was prepared by mixing the previous stock solution (20 µ1) with nitrogen-purged (10 min) 0.5 M sodium gluconate (400 µl). For labeling, an aliquot of water (100 µ1), an aliquot of the diluted stannous gluconate stock solution (20 µl), and an isotonic saline solution of $^{99m}TcO_4^-$ (500 µl, ~370 MBq) were added to a 1.5 ml microcentrifuge tube containing N_3S-Probestin (100 µg). The tube was vortexed for 30 sec and incubated at RT for 30 min. The ^{99m}TcO-N_3S-Probestin was purified by HPLC. The pure fraction was collected into 0.2 M sodium phosphate at pH - 8 (200 µl). The HPLC collected fraction was concentrated to ~200 µl by purging with nitrogen at 75 °C. The ^{99m}TcO-N_3S-Probestin conjugates were obtained in 50–60% radiochemical yield with >98% radiochemical purity after HPLC purification. The specific activity of the final product was not determined since the unlabeled N_3S-Probestin conjugate was efficiently separated from the product by HPLC. The ^{99m}TcO-N_3S-Probestin conjugates were characterized by comparing their HPLC retention time with corresponding Re(V) conjugates.

APN enzyme activity

Cell surface APN activity of intact cells was measured by a spectrophotometric assay as previously described using alanine *p*-nitroanilide (Ala-*p*NA) as a substrate for APN.[39] Assays were performed with intact confluent cell monolayers, grown in 96 well plates by plating about 5×10^4 cells/well. Cells were allowed to grow for 24 h followed by washing three times with PBS50. Cells were incubated with increasing concentrations (top dose of 1 mM) of bestatin or ReO-N_3S-Probestin conjugate in PBS50 (100 µl) and 2 mM Ala-*p*NA in PBS50 (100 µl) at RT for 30 min. The amount of *p*-nitroaniline formed was measured spectrophotometrically at 405 nm by ELx800™ Absorbance Microplate Reader (BioTek Instruments, Inc., Winooski, VT). Assays were run in triplicate, and cell-free and substrate-free blanks were run in parallel. EC_{50} values were calculated using GraphPad Prism 5 using non-linear regression (sigmoidal dose-response relation variable slope) analysis (GraphPad Software, La Jolla, CA).

HT-1080 tumor-bearing nude mice

The mice were housed five animals per cage in sterile micro isolator cages in a temperature- and humidity-controlled room with a 12-hour light/12-hour dark schedule. The animals were fed autoclaved rodent chow (Ralston Purina Company, St. Louis, MO) and water ad libitum. Animals were housed for an acclimation period of one week prior to inoculation of tumor

cells. The mice were anesthetized with 2% isoflurane (Baxter Healthcare Corp., Deerfield, IL) in oxygen at 2 L/min through a non-rebreathing anesthesia vaporizer.

Human fibrosarcoma xenografts were induced by subcutaneous injection of approximately 6.6×10^6 HT-1080 cells in a suspension of 50 μl sterile normal saline per injection site bilaterally into the subscapular region of mice. Two to three weeks after inoculation of the tumor cells, when the tumors reached 0.5 – 1 cm in diameter, the mice were recruited for biodistribution and SPECT imaging studies.

Biodistribution studies

Four HT-1080 tumor-bearing nude mice (22–24 g) were anesthetized with 2% isoflurane in oxygen at 2 L/min and injected with a dose of ^{99m}TcO-N_3S-PEG_2-Probestin (1.28 MBq) in 50 μl 0.2 M PBS (pH - 8) through the tail vein. The mice were euthanized and tissues/organs were excised at 1 hr post-injection (p.i.). The tissues/organs were washed with normal saline, dried by blotting on a tissue paper, and transferred to pre-weighed tubes. The tubes were weighed and radioactivity associated with each tissue was recorded on a Packard Cobra II automated gamma counter. Undiluted standard dose (8 μl) was counted along with the samples. All the data were corrected for ^{99m}Tc-decay. The percent injected dose (%ID) and percent injected dose per gram of tissue (%ID/g) for each tissue/organ was calculated. The total blood and muscle were estimated as 5.7% and 40% of the total body weight, respectively. The weight of stomach and intestines included their contents.

Planar imaging

HT-1080 tumor-bearing nude mice were anesthetized using 2% isoflurane in oxygen at 2 L/min, in a polypropylene induction chamber. When fully anesthetized, a dose of ^{99m}TcO-N_3S-PEG_2-Probestin (18.5 MBq) in 60 μl 0.2 M PBS (pH - 8) was injected through the tail vein. For the blocking experiment, a dose of ^{99m}TcO-N_3S-PEG_2-Probestin (24 MBq) in 70 μl 0.2 M PBS (pH - 8) along with 1 mg of ReO-N_3S-PEG_2-Probestin was injected. The mice were sacrificed at 1 hr p.i. and imaged in prone position using a parallel-hole collimator of the NanoSPECT camera. Static planar images with a frame size of 512 × 512 were acquired for 10 min. Planar images were visualized using InVivoScope™ (Bioscan, Washington, DC) software package.

SPECT imaging

HT-1080 tumor-bearing nude mice were anesthetized using 2% isoflurane in oxygen at 2 L/min, in a polypropylene induction chamber. When fully anesthetized, a dose of ^{99m}TcO-N_3S-PEG_2-Probestin (25.2 MBq) in 70 μl 0.2 M PBS (pH - 8) was injected through the tail vein. One mouse was sacrificed at 30 min and the other at 3 hr p.i. The mouse was placed on the mouse bed of the NanoSPECT camera and the SPECT imaging data were acquired in a helical scanning mode with 20 projections with an acquisition time of 60 s per projection. Raw SPECT data were reconstructed using HiSPECT (Bioscan, Washington, DC) software package. Reconstructed SPECT data were visualized using InVivoScope™ (Bioscan, Washington, DC) software package.

Results and Discussion

It is now widely accepted that angiogenesis is the rate-limiting step for the growth of solid tumors.[40–43] Antiangiogenesis therapy is currently being investigated around the world using recombinant antiangiogenic proteins, monoclonal antibodies, and various drugs.[44] These antiangiogenesis therapies have led to an increased interest in imaging as a means of monitoring therapeutic effect.[45, 46] Tumor angiogenesis imaging is intensively studied by targeting molecular markers of angiogenesis such as receptors, enzymes, integrins, or

extracellular matrix proteins. One of the most promising targets in this respect is integrin $\alpha_v\beta_3$, which has been successfully studied in patients and healthy volunteers by single photon emission computed tomography (SPECT) and positron emission tomography (PET) using Tc-99m and F-18 labeled RGD peptide conjugates.[47–50]

APN/CD13 is another potential target that could be exploited for imaging tumor angiogenesis. However, currently there is no targeting vector available for imaging APN/CD13 expression by using nuclear imaging techniques. We are exploring the possibility of using radiolabeled high affinity APN inhibitor conjugates as vectors to target APN/CD13 in vivo. We synthesized two probestin conjugates containing a N_3S chelator to enable Tc-99m labeling. We attached the chelator at C-terminus of the probestin since N-terminus is involved in binding with the enzyme, which preferentially releases amino acids from the N-terminal end of small peptides.[2] The N_3S-Probestin conjugates were manually synthesized by SPPS method employing traditional fmoc chemistry and HBTU activation of carboxyl groups on the reactant with the N-terminal amino group on the growing peptide anchored *via* the C-terminus to the resin (Figure 1). We used orthogonally-protected Lys or DAP (Fmoc-Lys(ivDde)-OH or Fmoc-DAP(ivDde)-OH) as they allow to build the tripeptide chelator sequence on the N-terminus of probestin. The 4-carbon side chain of the Lys residue acted as a spacer between the probestin and the chelator in N_3S-Probestin. Whereas, 8-amino-3,6-dioxaoctanoic acid (AEEA) acted as a linker between the probestin and the chelator in N_3S-PEG_2-Probestin. The ivDde group was selectively deprotected using 2% hydrazine in DMF. The N_3S-Probestin conjugates were obtained in an overall yield of 10–15% with >98% purity after HPLC purification. Mass spectral analyses were consistent with the molecular weights calculated for each conjugate (Table 1).

Tc-99m is a preferred radionuclide for SPECT due to its favorable nuclear properties (γ - 140.5 KeV, 89.1% abundance, half-life - 6.02 hr), lower cost, well-established radiochemistry, and availability.[51–53] Tetradentate tripeptide chelators of the N_3S type are frequently employed in the development of receptor-avid peptide based T-99m radiopharmaceuticals. For example, clinically used Acutect (Tc-99m Apcitide) and Neotect (Tc-99m Depreotide) radiopharmaceuticals (currently discontinued) were based on peptide targeting vectors linked to a tripeptide N_3S chelator.[54, 55] However, most tetradentate chelators containing a chiral carbon or an *N*-alkylated moiety produce diastereomers when a $[M(V)O]^{3+}$ (M = Tc, Re) core is bound to the donor groups in a square pyramidal coordination geometry as pendant groups are disposed in either *syn* or *anti* position relative to the M=O bond.[56–61] In our case, the tripeptide chelator sequence, DMG-Aaa-Cys (Aaa = Lys or DAP), is expected to form a neutral M(V)O-N_3S (M=^{99m}Tc, Re) complex with the loss of three protons of the donor groups (the amide proton of Lys or DAP and the amide and thiol protons of Cys), while the tertiary amine of DMG is expected to coordinate to the $[M(V)O]^{3+}$ core through its lone pair of electrons and form a coordinate bond with the metal.

Cold Re-complexation was achieved by reacting N_3S-Probestin with an excess of Re(V)-gluconate synthon. Re conjugate was expected to present as two peaks on the HPLC chromatogram due to the formation of syn and anti conformations of Lys or DAP side chain with respect to the M=O bond. However, HPLC analysis of the reaction mixture revealed a broad peak indicative of formation of the diastereomers appearing as a merged single peak under our HPLC conditions (Figure 2). Mass spectral analyses of the Re conjugates were consistent with the formation of neutral Re(V)O-N_3S complexes (Table 1). ReO-N_3S-Probestin conjugates were obtained in 50–75% yield after HPLC purification.

Radiolabeling of N_3S-Probestin conjugates with Tc-99m was performed by transmetallation using ^{99m}Tc(V) gluconate synthon as previously described (Figure 1).[38] The HPLC

retention times of ^{99m}Tc(V)-labeled probestin conjugates were matched to the corresponding cold Re(V) conjugates, which confirmed the formation of the radiolabeled product. The HPLC chromatograms in Figures 2 show the elution profiles of the N_3S-PEG_2-Probestin conjugate and its Re(V) and ^{99m}Tc(V) complexes. The figure also shows that both the Re- and Tc-99m conjugates were eluted at 14.3 min. The ^{99m}TcO-N_3S-PEG_2-Probestin conjugate eluted ~1 min after the unlabeled N_3S-PEG_2-Probestin conjugate under our HPLC conditions enabling the collection of high-specific activity, essentially carrier-free ^{99m}TcO-N_3S-PEG_2-Probestin. The radiochemical purity of the HPLC-purified product was found to be >98%.

Initial biological activity of ReO-N_3S-Probestin conjugates was determined by performing an in vitro APN enzyme assay using intact HT-1080 cells and Ala-*p*NA as APN substrate with EC_{50} values determined using non-linear regression analysis. The results of the experiments (Figure 3) demonstrated higher inhibition of APN enzyme activity by ReO-N_3S-Probestin conjugates when compared to bestatin, a known slow-binding competitive inhibitor of APN.[62] The EC_{50} values were determined to be 979.2, 39.6, and 23.6 μM for bestatin, ReO-N_3S-Probestin, and ReO-N_3S-PEG_2-Probestin respectively. Results obtained from these in vitro APN enzyme activity assay conforms that the attachment of a chelator at C-terminus of probestin does not affect its ability to bind the enzymatic active site of APN.

In vivo biodistribution studies of ^{99m}TcO-N_3S-PEG_2-Probestin were performed in nude mice xenografted in their mid-flanks with human fibrosarcoma tumors derived from HT-1080 cells. The selection of ^{99m}TcO-N_3S-PEG_2-Probestin for in vivo evaluation was based on two reasons: 1) it demonstrated slightly better EC_{50} value than ^{99m}TcO-N_3S-Probestin, and 2) it was relatively more hydrophilic than ^{99m}TcO-N_3S-Probestin (HPLC retention times differ by >1 min, Table 1). In general, increasing hydrophilic character of a small peptide conjugate increases its clearance via renal-urinary pathway, which is preferable for the rapid clearance of background signals in images. Results obtained at 1 hr p.i. are summarized in Table 2. A tumor uptake value of 2.88 ± 0.64 %ID/g and a low residual radioactivity of 0.60 ± 0.33 %ID/g in blood yielded tumor-to-blood and tumor-to-muscle ratios of approximately 4.8 and 5.3 respectively. These results indicate fast clearance of ^{99m}TcO-N_3S-PEG_2-Probestin from the bloodstream. High uptake values in kidney, liver, and intestine of 48.0 ± 3.4 %ID/g, 12.0 ± 0.8 %ID/g, and 4.8 ± 0.3 %ID/g respectively indicates that ^{99m}TcO-N_3S-PEG_2-Probestin is eliminated from the body *via* renal and hepatobiliary clearance pathways. However, it is unclear from these results that the radioactivity uptake is due to normal metabolism of ^{99m}TcO-N_3S-PEG_2-Probestin or specific uptake by tissue-associated APN expression. It is known that APN is highly expressed on the renal proximal tubules, brush border membranes of the small intestine, and liver.[4, 63]

Planar images of HT-1080 tumor-bearing nude mice injected with ^{99m}TcO-N_3S-PEG_2-Probestin alone or along with a large excess of ReO-N_3S-PEG_2-Probestin to block APN active sites obtained at 1 hr p.i. are shown in Figure 4 and Figure 5a. The 1 hr p.i. whole body planar image of the unblocked mouse demonstrates increased uptake in the tumor sites, thymus, kidneys, liver, and intestine in descending level of intensity relative to the background soft tissues (Figure 4). The 1 hr p.i. whole body planar image of the APN-blocked mouse reveals no significant radiotracer uptake in the tumor sites, thymus, or kidneys (Figure 4). There is relatively increased radioactivity in the liver and intestine in the APN-blocked mouse compared to the unblocked mouse (Figure 5a). The negligible uptake of radioactivity in the tumor sites, thymus, and kidneys suggests adequate blockade of the APN in those tissue/organs, and the radioactivity uptake seen in the unblocked mouse is APN-specific. The relatively increased radioactivity in the liver and intestine is consistent with the increased radioactivity excretion via the hepatobiliary and GI tract in APN-blocked

mouse. Secondary to the increased excretory activity in the hepatobiliary and GI tract, the APN blockade in the liver and intestinal lining is likely masked.

Early and delayed SPECT images of HT-1080 tumor-bearing mice injected with ^{99m}TcO-N_3S-PEG_2-Probestin (Figure 5b and 5c, respectively) were obtained at 30 min p.i. (early) and at 3 hr p.i. (delayed). The early SPECT images, MIP and transverse views (Figure 5b), reveal intense radioactivity in the kidneys with significantly less radioactivity in the intestine. Intense radioactivity was also noted in the urinary bladder as radioactive urine is excreted from the kidneys into the urinary bladder. Delayed SPECT images, MIP and transverse views (Figure 5c), demonstrates background radioactivity in the kidneys with intensity level similar to that of blood radioactivity seen in the aorta. Unlike the observation made in the early SPECT images, the delayed SPECT images show intense radioactivity in the intestine compared to the radioactivity in the kidneys, which is essentially at background/blood level. Decreased radioactivity in the kidneys and tumor sites on delayed SPECT images relative to early SPECT images is suggestive of reversible binding of ^{99m}TcO-N_3S-PEG_2-Probestin to APN. Reversible binding is taken as binding of ^{99m}TcO-N_3S-PEG_2-Probestin to APN for a short-time period (< 3 hr) and then detaching from APN as an intact molecule without any internalization. Although the reversible binding of ^{99m}TcO-N_3S-PEG_2-Probestin to APN may not be desirable for delayed imaging, it may be very useful for early phase imaging studies especially when used with short-lived radionuclides. Radioactivity seen in the urinary bladder on both SPECT MIP images (Figure 5b and 5c) demonstrates the presence of urinary excretion in addition to GI tract excretion of radioactivity, which confirms the results obtained from the biodistribution studies.

The HPLC analysis of urine samples collected during the imaging studies from HT-1080 tumor-bearing nude mice injected with ^{99m}TcO-N_3S-PEG_2-Probestin showed that the radiotracer is excreted intact (Figure 2). This result further suggests the reversible binding of ^{99m}TcO-N_3S-PEG_2-Probestin to APN and that this agent is eliminated via glomerular filtration when released from APN sites in kidneys as it is a low molecular weight hydrophilic and neutral compound.

The ^{99m}TcO-N_3S-PEG_2-Probestin evaluated in this study is a first-generation conjugate. Further improvements in the structure of the conjugate may improve its tumor uptake and make it an attractive candidate for imaging APN expression in vivo. One strategy that has been successfully applied to improve tumor uptake of the radiolabeled cyclic RGD peptide conjugates is to have multiple RGD units in the conjugate.[64, 65] Apparently, a multimeric preparation significantly enhances the binding affinity of the receptor-ligand interaction through the polyvalency effect.[64, 66] Together with the choice of appropriate linker for desired pharmacokinetics, it may be possible to exploit multimerization approach for enhanced tumor uptake of the probestin motif via APN-targeting.

Due to high abdominal uptake, as seen with ^{99m}TcO-N_3S-PEG_2-Probestin, the potential application of APN-targeted radiotracers could be envisaged for imaging primary tumors that are outside of the abdomen. Particularly, when SPECT/CT is employed for anatomic localization, the separation of physiologic activity in the abdominal organs versus tumor activity could be possible. Thus, APN-targeted radiotracers may find potential application for imaging breast and lung tumor angiogenesis.

Conclusions

We have successfully synthesized and evaluated the first generation ^{99m}Tc-labeled probestin conjugates. The in vitro APN enzymatic studies performed in human fibrosarcoma HT-1080 cells showed that ReO-N_3S-Probestin conjugates are more effective inhibitors than bestatin.

The in vivo biodistribution and imaging studies of ^{99m}TcO-N_3S-PEG_2-Probestin in nude mice xenografted with HT-1080 human fibrosarcoma tumors showed high radioactivity uptake in tumors coupled with rapid elimination of the radioactivity from the blood stream *via* the renal and the hepatobiliary clearance pathways. The image findings collectively demonstrate the radiotracer uptake is APN-specific and suggests reversible binding of ^{99m}TcO-N_3S-PEG_2-Probestin to APN active sites, particularly in the kidneys. The results of these studies demonstrate the feasibility of using probestin as a vector for targeting APN in vivo and provide a foundation for the development of novel APN-targeted radiotracers with a potential application in imaging tumor angiogenesis.

Acknowledgments

This work was funded by the American Cancer Society IRG Seed Grant C5052202 and the OU College of Pharmacy Startup Grant. We acknowledge funding from the NIH grant S10RR025652 for the NanoSPECT system. We acknowledge the OU Nuclear Pharmacy for providing Tc-99m. We gratefully acknowledge the assistance of Dr. Vivek Yadav during tumor cell inoculation and Mr. Kaustav Sahoo for operating the NanoSPECT system.

References

1. Look AT, Ashmun RA, Shapiro LH, Peiper SC. Human myeloid plasma membrane glycoprotein CD13 (gp150) is identical to aminopeptidase N. J Clin Invest. 1989; 83:1299–1307. [PubMed: 2564851]
2. Sjostrom H, Noren O, Olsen J. Structure and function of aminopeptidase N. Adv Exp Med Biol. 2000; 477:25–34. [PubMed: 10849727]
3. Shipp M, Look A. Hematopoietic differentiation antigens that are membrane-associated enzymes: cutting is the key! Blood. 1993; 82:1052–1070. [PubMed: 8102558]
4. Dixon J, Kaklamanis L, Turley H, Hickson ID, Leek RD, Harris AL, Gatter KC. Expression of aminopeptidase-n (CD 13) in normal tissues and malignant neoplasms of epithelial and lymphoid origin. Journal of Clinical Pathology. 1994; 47:43–47. [PubMed: 7907609]
5. Kenny AJ, Maroux S. Topology of microvillar membrance hydrolases of kidney and intestine. Physiological Reviews. 1982; 62:91–128. [PubMed: 6119713]
6. Tokuhara T, Hattori N, Ishida H, Hirai T, Higashiyama M, Kodama K, Miyake M. Clinical significance of aminopeptidase N in non-small cell lung cancer. Clin Cancer Res. 2006; 12:3971–3978. [PubMed: 16818694]
7. Hashida H, Takabayashi A, Kanai M, Adachi M, Kondo K, Kohno N, Yamaoka Y, Miyake M. Aminopeptidase N is involved in cell motility and angiogenesis: its clinical significance in human colon cancer. Gastroenterology. 2002; 122:376–386. [PubMed: 11832452]
8. Ishii K, Usui S, Sugimura Y, Yoshida S, Hioki T, Tatematsu M, Yamamoto H, Hirano K. Aminopeptidase N regulated by zinc in human prostate participates in tumor cell invasion. Int J Cancer. 2001; 92:49–54. [PubMed: 11279605]
9. Wickström M, Larsson R, Nygren P, Gullbo J. Aminopeptidase N (CD13) as a target for cancer chemotherapy. Cancer Science. 2011; 102:501–508. [PubMed: 21205077]
10. Menrad A, Speicher D, Wacker J, Herlyn M. Biochemical and Functional Characterization of Aminopeptidase N Expressed by Human Melanoma Cells. Cancer Research. 1993; 53:1450–1455. [PubMed: 8095183]
11. Saiki I, Yoneda J, Azuma I, Fujii H, Abe F, Nakajima M, Tsuruo T. Role of aminopeptidase N (CD13) in tumor-cell invasion and extracellular matrix degradation. International Journal of Cancer. 1993; 54:137–143.
12. Fujii H, Nakajima M, Saiki I, Yoneda J, Azuma I, Tsuruo T. Human melanoma invasion and metastasis enhancement by high expression of aminopeptidase N/CD13. Clinical and Experimental Metastasis. 1995; 13:337–344. [PubMed: 7641419]
13. Pasqualini R, Koivunen E, Kain R, Lahdenranta J, Sakamoto M, Stryhn A, Ashmun RA, Shapiro LH, Arap W, Ruoslahti E. Aminopeptidase N is a receptor for tumor-homing peptides and a target for inhibiting angiogenesis. Cancer Res. 2000; 60:722–727. [PubMed: 10676659]

14. Bhagwat SV, Lahdenranta J, Giordano R, Arap W, Pasqualini R, Shapiro LH. CD13/APN is activated by angiogenic signals and is essential for capillary tube formation. Blood. 2001; 97:652–659. [PubMed: 11157481]
15. Zhang Z, Hatta H, Ito T, Nishimoto S. Synthesis and photochemical properties of photoactivated antitumor prodrugs releasing 5-fluorouracil. Org Biomol Chem. 2005; 3:592–596. [PubMed: 15703793]
16. Ndinguri MW, Solipuram R, Gambrell RP, Aggarwal S, Hammer RP. Peptide Targeting of Platinum Anti-Cancer Drugs. Bioconjugate Chemistry. 2009; 20:1869–1878. [PubMed: 19775102]
17. van Laarhoven HW, Gambarota G, Heerschap A, Lok J, Verhagen I, Corti A, Toma S, Gallo Stampino C, van der Kogel A, Punt CJ. Effects of the tumor vasculature targeting agent NGR-TNF on the tumor microenvironment in murine lymphomas. Invest New Drugs. 2006; 24:27–36. [PubMed: 16379040]
18. Zhang Z, Harada H, Tanabe K, Hatta H, Hiraoka M, Nishimoto S. Aminopeptidase N/CD13 targeting fluorescent probes: synthesis and application to tumor cell imaging. Peptides. 2005; 26:2182–2187. [PubMed: 15885853]
19. Moffatt S, Wiehle S, Cristiano RJ. Tumor-specific gene delivery mediated by a novel peptide-polyethylenimine-DNA polyplex targeting aminopeptidase N/CD13. Hum Gene Ther. 2005; 16:57–67. [PubMed: 15703489]
20. van Hensbergen Y, Broxterman HJ, Elderkamp YW, Lankelma J, Beers JC, Heijn M, Boven E, Hoekman K, Pinedo HM. A doxorubicin-CNGRC-peptide conjugate with prodrug properties. Biochem Pharmacol. 2002; 63:897–908. [PubMed: 11911842]
21. Curnis F, Sacchi A, Borgna L, Magni F, Gasparri A, Corti A. Enhancement of tumor necrosis factor alpha antitumor immunotherapeutic properties by targeted delivery to aminopeptidase N (CD13). Nat Biotechnol. 2000; 18:1185–1190. [PubMed: 11062439]
22. Arap W, Pasqualini R, Ruoslahti E. Cancer treatment by targeted drug delivery to tumor vasculature in a mouse model. Science. 1998; 279:377–380. [PubMed: 9430587]
23. Zhang Z, Hatta H, Tanabe K, Nishimoto S. A new class of 5-fluoro-2'-deoxyuridine prodrugs conjugated with a tumor-homing cyclic peptide CNGRC by ester linkers: synthesis, reactivity, and tumor-cell-selective cytotoxicity. Pharm Res. 2005; 22:381–389. [PubMed: 15835743]
24. von Wallbrunn A, Waldeck J, Holtke C, Zuhlsdorf M, Mesters R, Heindel W, Schafers M, Bremer C. In vivo optical imaging of CD13/APN-expression in tumor xenografts. J Biomed Opt. 2008; 13:011007. [PubMed: 18315356]
25. Oostendorp M, Douma K, Hackeng TM, Dirksen A, Post MJ, van Zandvoort MAMJ, Backes WH. Quantitative Molecular Magnetic Resonance Imaging of Tumor Angiogenesis Using cNGR-Labeled Paramagnetic Quantum Dots. Cancer Res. 2008; 68:7676–7683. [PubMed: 18794157]
26. Ellerby HM, Bredesen DE, Fujimura S, John V. Hunter-Killer Peptide (HKP) for Targeted Therapy. J Med Chem. 2008; 51:5887–5892. [PubMed: 18828573]
27. Gregorc V, Zucali PA, Santoro A, Ceresoli GL, Citterio G, De Pas TM, Zilembo N, De Vincenzo F, Simonelli M, Rossoni G, Spreafico A, Grazia Vigano M, Fontana F, De Braud FG, Bajetta E, Caligaris-Cappio F, Bruzzi P, Lambiase A, Bordignon C. Phase II Study of Asparagine-Glycine-Arginine-Human Tumor Necrosis Factor {alpha}, a Selective Vascular Targeting Agent, in Previously Treated Patients With Malignant Pleural Mesothelioma. J Clin Oncol. 2010; 28:2604–2611. [PubMed: 20406925]
28. Curnis F, Longhi R, Crippa L, Cattaneo A, Dondossola E, Bachi A, Corti A. Spontaneous Formation of L-Isoaspartate and Gain of Function in Fibronectin. J Biol Chem. 2006; 281:36466–36476. [PubMed: 17015452]
29. Curnis F, Sacchi A, Gasparri A, Longhi R, Bachi A, Doglioni C, Bordignon C, Traversari C, Rizzardi G-P, Corti A. Isoaspartate-Glycine-Arginine: A New Tumor Vasculature-Targeting Motif. Cancer Res. 2008; 68:7073–7082. [PubMed: 18757422]
30. Spitaleri A, Mari S, Curnis F, Traversari C, Longhi R, Bordignon C, Corti A, Rizzardi G-P, Musco G. Structural Basis for the Interaction of isoDGR with the RGD-binding Site of {alpha}v{beta}3 Integrin. J Biol Chem. 2008; 283:19757–19768. [PubMed: 18480047]
31. Curnis F, Cattaneo A, Longhi R, Sacchi A, Gasparri AM, Pastorino F, Di Matteo P, Traversari C, Bachi A, Ponzoni M, Rizzardi G-P, Corti A. Critical role of flanking residues in NGR-to-isoDGR

transition and CD13/Integrin receptor switching. J Biol Chem. 2010; 285:9114–9123. [PubMed: 20064928]

32. Corti A, Curnis F, Arap W, Pasqualini R. The neovasculature homing motif NGR: more than meets the eye. Blood. 2008; 112:2628–2635. [PubMed: 18574027]
33. Pathuri G, Sahoo K, Awasthi V, Gali H. Synthesis and in vivo evaluation of Tc-99m-labeled cyclic CisoDGRC peptide conjugates for targeting [alpha]v[beta]3 integrin expression. Bioorganic & Medicinal Chemistry Letters. 2010; 20:5969–5972. [PubMed: 20829039]
34. Plesniak LA, Salzameda B, Hinderberger H, Regan E, Kahn J, Mills SA, Teriete P, Yao Y, Jennings P, Marassi F, Adams JA. Structure and Activity of CPNGRC: A Modified CD13/APN Peptidic Homing Motif. Chemical Biology & Drug Design. 2010; 75:551–562. [PubMed: 20374250]
35. Aoyagi T, Yoshida S, Nakamura Y, Shigihara Y, Hamada M, Takeuchi T. Probestin, a new inhibitor of aminopeptidase M, produced by Streptomyces azureus MH663-2F6I. Taxonomy, production, isolation, physico-chemical properties and biological activities. J Antibiot (Tokyo). 1990; 43:143–148. [PubMed: 1968900]
36. Itoh Y, Ishikawa M, Naito M, Hashimoto Y. Protein Knockdown Using Methyl Bestatin–Ligand Hybrid Molecules: Design and Synthesis of Inducers of Ubiquitination-Mediated Degradation of Cellular Retinoic Acid-Binding Proteins. Journal of the American Chemical Society. 2010; 132:5820–5826. [PubMed: 20369832]
37. Noll B, Kniess T, Friebe M, Spies H, Johannsen B. Rhenium(V) Gluconate, a Suitable Precursor for the Preparation of Rhenium(V) Complexes. Isotopes in Environmental and Health Studies. 1996; 32:21–29.
38. Smith CJ, Gali H, Sieckman GL, Higginbotham C, Volkert WA, Hoffman TJ. Radiochemical investigations of (99m)Tc-N(3)S-X-BBN[7–14]NH(2): an in vitro/in vivo structure-activity relationship study where X = 0- 3- 5- 8-, and 11-carbon tethering moieties. Bioconjug Chem. 2003; 14:93–102. [PubMed: 12526698]
39. Ashmun R, Look A. Metalloprotease activity of CD13/aminopeptidase N on the surface of human myeloid cells. Blood. 1990; 75:462–469. [PubMed: 1967220]
40. Folkman J. Angiogenesis in cancer, vascular, rheumatoid and other disease. Nat Med. 1995; 1:27–31. [PubMed: 7584949]
41. Hanahan D, Folkman J. Patterns and emerging mechanisms of the angiogenic switch during tumorigenesis. Cell. 1996; 86:353–364. [PubMed: 8756718]
42. Plate KH, Breier G, Risau W. Molecular mechanisms of developmental and tumor angiogenesis. Brain Pathol. 1994; 4:207–218. [PubMed: 7524960]
43. Folkman J. Tumor angiogenesis: therapeutic implications. N Engl J Med. 1971; 285:1182–1186. [PubMed: 4938153]
44. Folkman J. Angiogenesis: an organizing principle for drug discovery? Nat Rev Drug Discov. 2007; 6:273–286. [PubMed: 17396134]
45. Beer AJ, Wester H-J, Schwaiger M. Molecular Imaging of Angiogenesis. 2010:105–115.
46. Hsu AR, Chen X. Advances in Anatomic, Functional, and Molecular Imaging of Angiogenesis. J Nucl Med. 2008; 49:511–514. [PubMed: 18375921]
47. Kenny LM, Coombes RC, Oulie I, Contractor KB, Miller M, Spinks TJ, McParland B, Cohen PS, Hui A-M, Palmieri C, Osman S, Glaser M, Turton D, Al-Nahhas A, Aboagye EO. Phase I Trial of the Positron-Emitting Arg-Gly-Asp (RGD) Peptide Radioligand 18F-AH111585 in Breast Cancer Patients. J Nucl Med. 2008; 49:879–886. [PubMed: 18483090]
48. Bach-Gansmo T, Danielsson R, Saracco A, Wilczek B, Bogsrud TV, Fangberget A, Tangerud A, Tobin D. Integrin receptor imaging of breast cancer: a proof-of-concept study to evaluate 99mTc-NC100692. J Nucl Med. 2006; 47:1434–1439. [PubMed: 16954550]
49. Beer AJ, Niemeyer M, Carlsen J, Sarbia M, Nahrig J, Watzlowik P, Wester H-J, Harbeck N, Schwaiger M. Patterns of {alpha}v{beta}3 Expression in Primary and Metastatic Human Breast Cancer as Shown by 18F-Galacto-RGD PET. J Nucl Med. 2008; 49:255–259. [PubMed: 18199623]
50. Mittra ES, Goris ML, Iagaru AH, Kardan A, Burton L, Berganos R, Chang E, Liu S, Shen B, Chin FT, Chen X, Gambhir SS. Pilot pharmacokinetic and dosimetric studies of (18)F-FPPRGD2: a

PET radiopharmaceutical agent for imaging alpha(v)beta(3) integrin levels. Radiology. 2011; 260:182–191. [PubMed: 21502381]

51. Arano Y. Recent advances in Tc-99m radiopharmaceuticals. Annals of Nuclear Medicine. 2002; 16:79–93. [PubMed: 12043913]
52. Jurisson SS, Lydon JD. Potential Technetium Small Molecule Radiopharmaceuticals. Chemical Reviews. 1999; 99:2205–2218. [PubMed: 11749479]
53. Bartholoma MD, Louie AS, Valliant JF, Zubieta J. Technetium and Gallium Derived Radiopharmaceuticals: Comparing and Contrasting the Chemistry of Two Important Radiometals for the Molecular Imaging Era. Chemical Reviews. 2010; 110:2903–2920. [PubMed: 20415476]
54. Francesconi LC, Zheng Y, Bartis J, Blumenstein M, Costello C, De Rosch MA. Preparation and Characterization of [99TcO] Apcitide: A Technetium Labeled Peptide. Inorganic Chemistry. 2004; 43:2867–2875. [PubMed: 15106974]
55. Cyr JE, Pearson DA, Nelson CA, Lyons BA, Zheng Y, Bartis J, He J, Cantorias MV, Howell RC, Francesconi LC. Isolation, Characterization, and Biological Evaluation of Syn and Anti Diastereomers of [99mTc]Technetium Depreotide: a Somatostatin Receptor Binding Tumor Imaging Agent. Journal of Medicinal Chemistry. 2007; 50:4295–4303. [PubMed: 17691760]
56. Cantorias MV, Howell RC, Todaro L, Cyr JE, Berndorff D, Rogers RD, Francesconi LC. MO Tripeptide Diastereomers (M = 99/99mTc, Re): Models To Identify the Structure of 99mTc Peptide Targeted Radiopharmaceuticals. Inorganic Chemistry. 2007; 46:7326–7340. [PubMed: 17691766]
57. Wong E, Fauconnier T, Bennett S, Valliant J, Nguyen T, Lau F, Lu LFL, Pollak A, Bell RA, Thornback JR. Rhenium(V) and Technetium(V) Oxo Complexes of an N2N'S Peptidic Chelator: Evidence of Interconversion between the Syn and Anti Conformations. Inorganic Chemistry. 1997; 36:5799–5808. [PubMed: 11670202]
58. Francesconi LC, Graczyk G, Wehrli S, Shaikh SN, McClinton D, Liu S, Zubieta J, Kung HF. Synthesis and characterization of neutral MVO (M = technetium, rhenium) amine-thiol complexes containing a pendant phenylpiperidine group. Inorganic Chemistry. 1993; 32:3114–3124.
59. Lever SZ, Baidoo KE, Mahmood A. Structure proof of syn/anti isomerism in N-alkylated diaminedithiol (DADT) complexes of technetium. Inorganica Chimica Acta. 1990; 176:183–184.
60. Valliant JF, Riddoch RW, Hughes DW, Roe DG, Fauconnier TK, Thornback JR. The solid phase synthesis and NMR spectroscopy of a 99Tc chelate-bombesin derived peptide conjugate. Inorganica Chimica Acta. 2001; 325:155–163.
61. Wong E, Bennett S, Lawrence B, Fauconnier T, Lu LFL, Bell RA, Thornback JR, Eshima D. Tuftsin Receptor-Binding Peptide Labeled with Technetium: Chemistry and Preliminary in Vitro Receptor-Binding Study. Inorganic Chemistry. 2001; 40:5695–5700. [PubMed: 11599972]
62. Bauvois B, Dauzonne D. Aminopeptidase-N/CD13 (EC 3.4.11.2) inhibitors: chemistry, biological evaluations, and therapeutic prospects. Med Res Rev. 2006; 26:88–130. [PubMed: 16216010]
63. Stange T, Kettmann U, Holzhausen HJ. Immunoelectron microscopic single and double labelling of aminopeptidase N (CD 13) and dipeptidyl peptidase IV (CD 26). Acta Histochem. 1996; 98:323–331. [PubMed: 8863861]
64. Li, Z-b; Cai, W.; Cao, Q.; Chen, K.; Wu, Z.; He, L.; Chen, X. 64Cu-Labeled Tetrameric and Octameric RGD Peptides for Small-Animal PET of Tumor {alpha}v{beta}3 Integrin Expression. J Nucl Med. 2007; 48:1162–1171. [PubMed: 17574975]
65. Liu S. Radiolabeled Cyclic RGD Peptides as Integrin αvβ3-Targeted Radiotracers: Maximizing Binding Affinity via Bivalency. Bioconjug Chem. 2009; 20:2199–2213. [PubMed: 19719118]
66. Mammen M, Choi SK, Whitesides GM. Polyvalent interactions in biological systems: Implications for design and use of multivalent ligands and inhibitors. Angewandte Chemie-International Edition. 1998; 37:2755–2794.

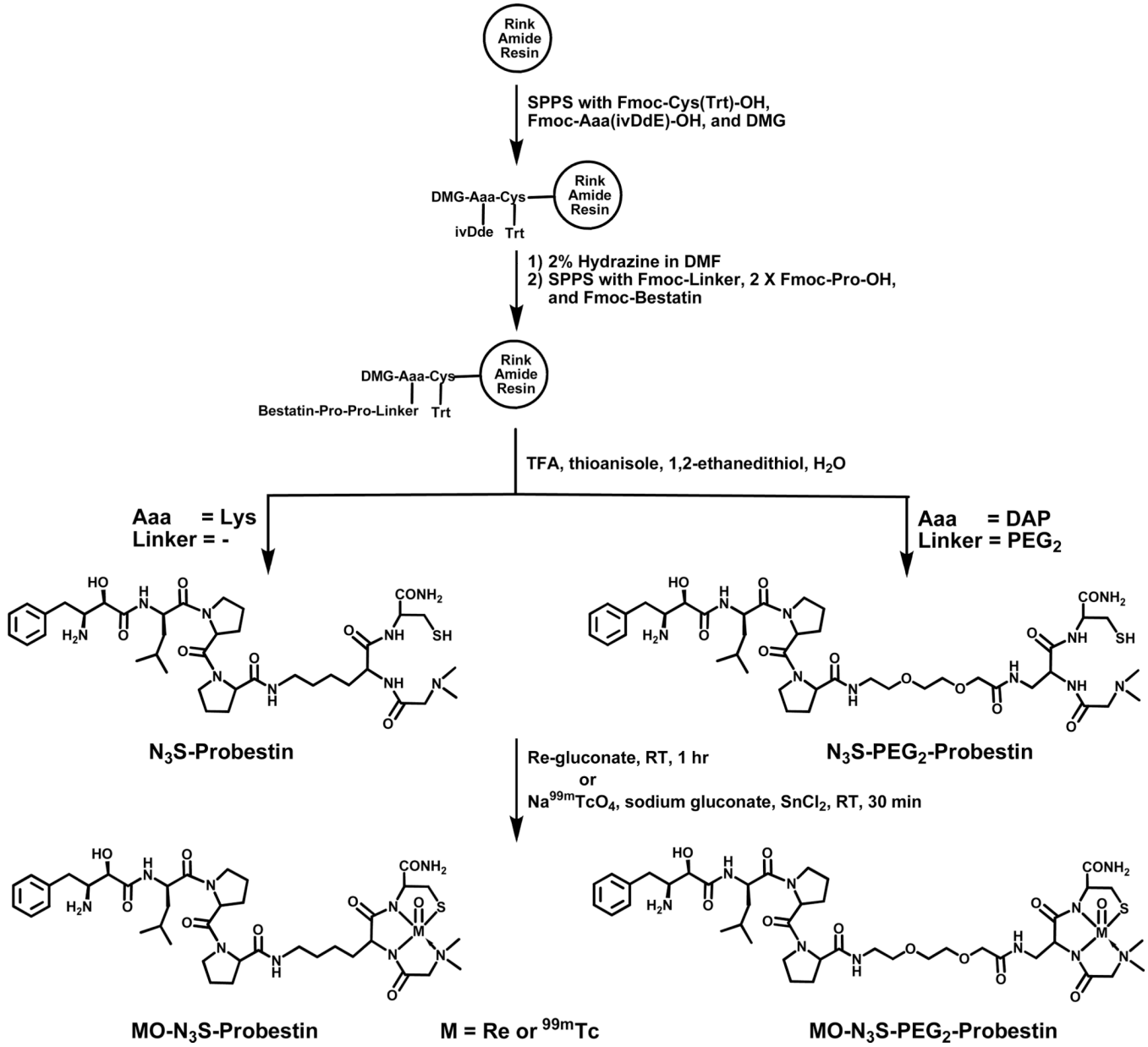

Figure 1.

Synthesis and complexation of N_3S-Probestin conjugates with $[Re/^{99m}Tc(V)O]^{3+}$-core.

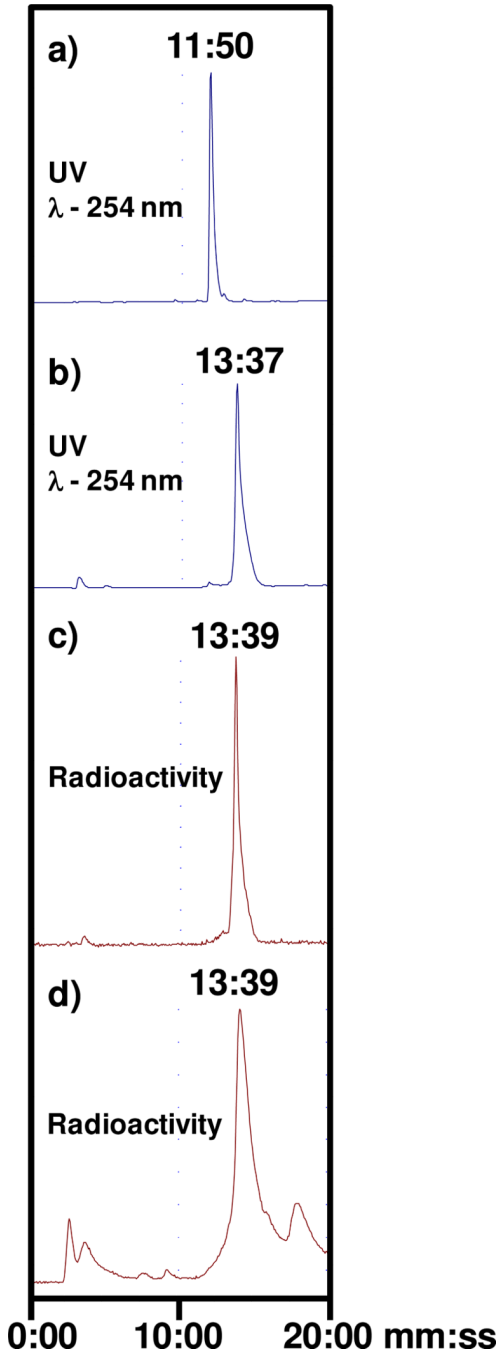

Figure 2.

Radio-HPLC chromatograms of a) N_3S-PEG_2-Probestin, b) ReO-N_3S-PEG_2-Probestin, c) ^{99m}TcO-N_3S-PEG_2-Probestin, and d) mouse urine collected at 10 min p.i. of ^{99m}TcO-N_3S-PEG_2-Probestin.

	Bestatin	ReO-N_3S-Probestin	ReO-N_3S-PEG_2-Probestin
Hill Slope	-0.41	-0.38	-0.46
EC_{50} (μM)	979.2	41.4	23.6

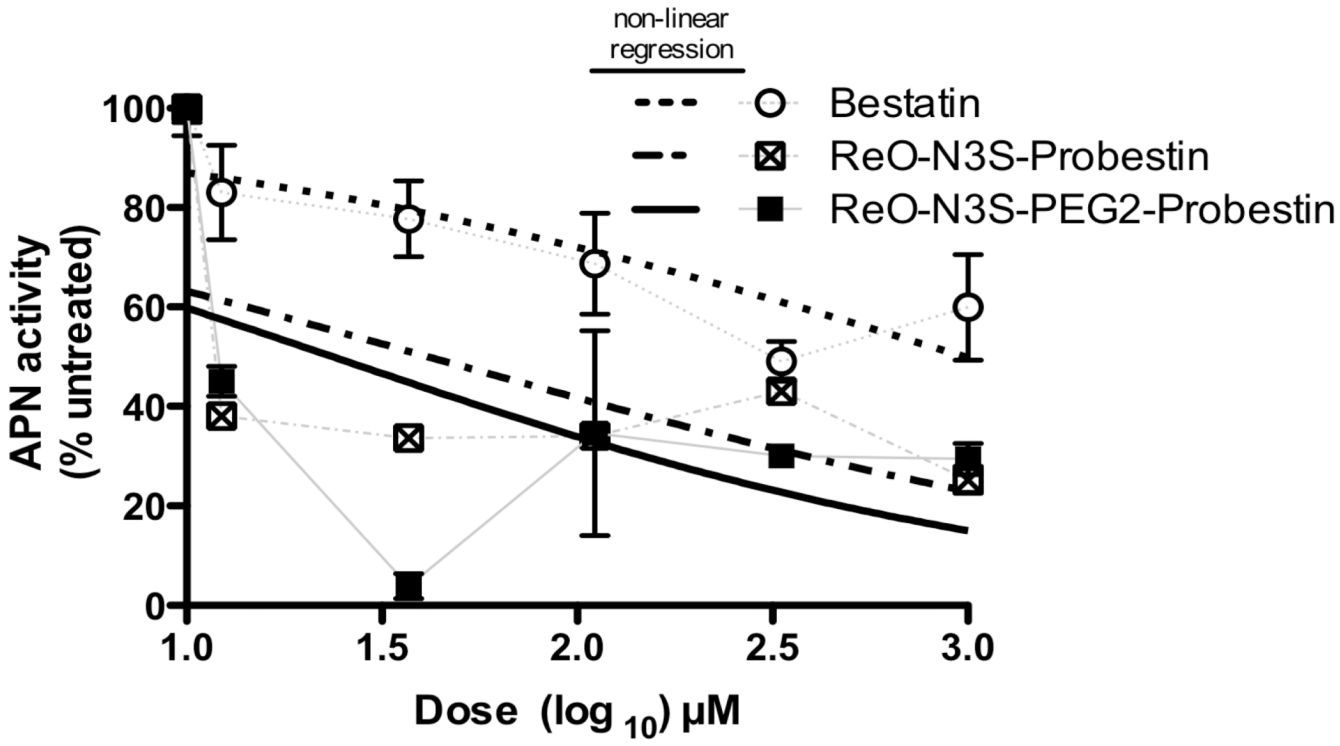

Figure 3.

Enzyme activity of APN present on HT-1080 cells in the presence of increasing concentrations of bestatin or ReO-N_3S-Probestin conjugates. The enzyme activity was estimated by measuring the absorbance at 405 nm of *p*-nitroaniline formed by the hydrolysis of L-alanine-*p*-nitroanilide (substrate) at room temperature in 30 min. EC_{50} values were calculated by non-linear regression (dose-response, variable slope) analysis using GraphPad Prism.

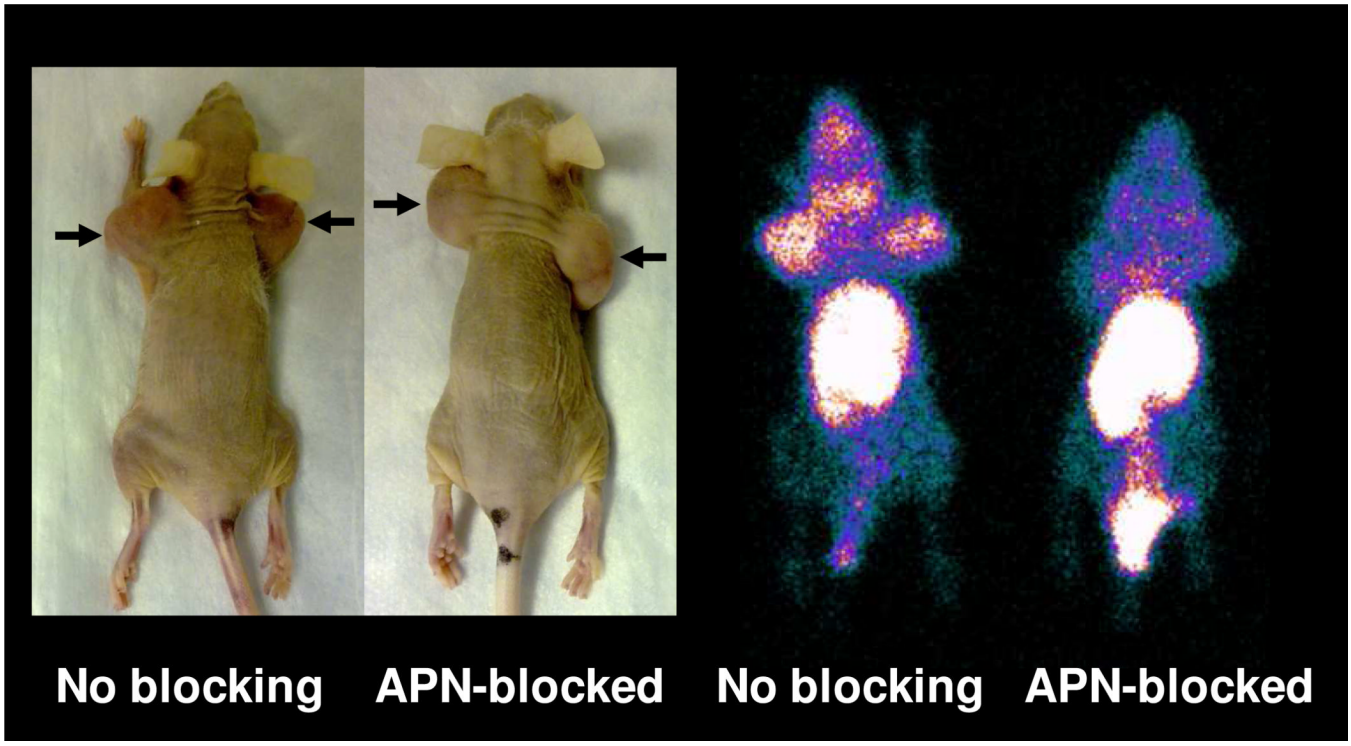

Figure 4.

Photograph of the HT-1080 tumor-bearing nude mice used for imaging with ^{99m}TcO-N_3S-PEG_2-Probestin (arrows indicate tumor) and whole body planar images of the same mice at 1 hr p.i. ReO-N_3S-PEG_2-Probestin (1 mg) was co-injected intravenously along with the ^{99m}TcO-N_3S-PEG_2-Probestin for blocking APN specific uptake of the radioactivity. Planar images were acquired in prone position.

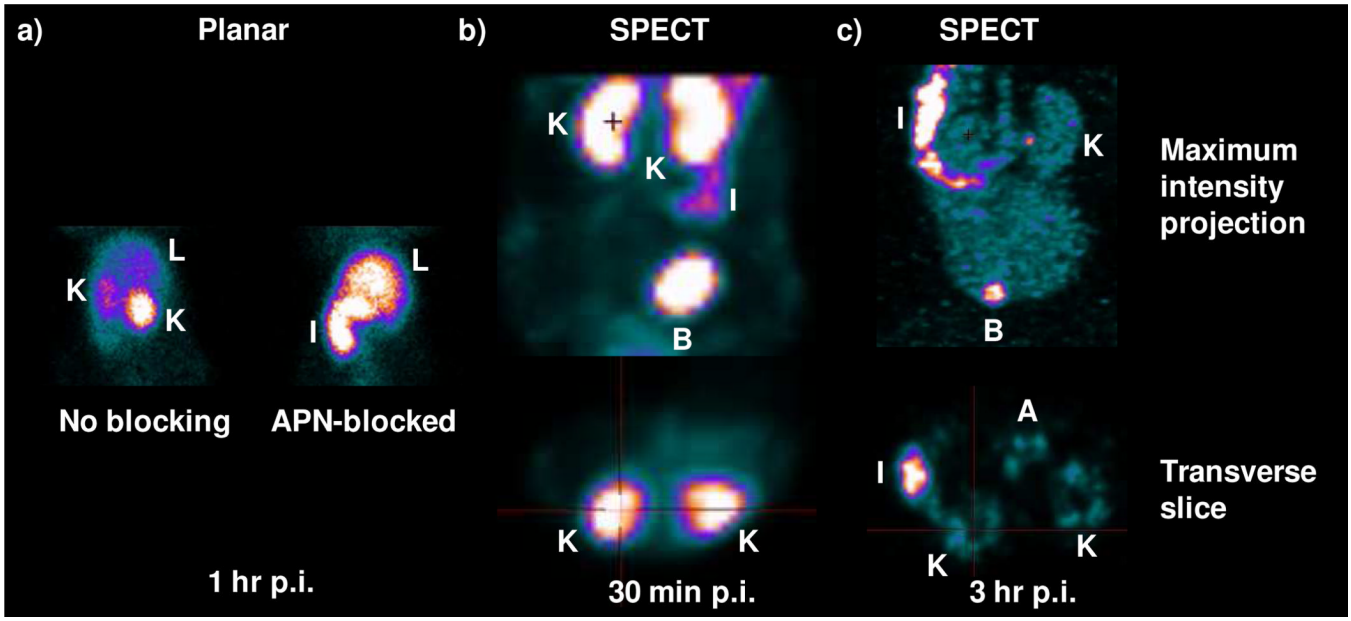

Figure 5.

(a) Abdomen planarimages of the HT-1080 tumor-bearing nude mice injected with ^{99m}TcO-N_3S-PEG_2-Probestin at 1 hr p.i. ReO-N_3S-PEG_2-Probestin (1 mg) was co-injected intravenously along with the ^{99m}TcO-N_3S-PEG_2-Probestin for blocking APN specific uptake of the radioactivity. Planar images were acquired in prone position. (b) Early and (c) delayed abdomen SPECT images of a HT-1080 tumor-bearing nude mouse injected with ^{99m}TcO-N_3S-PEG_2-Probestin. Labels: K - kidney; L - Liver; I - Intestine; B - Bladder.

TABLE 1

HPLC and mass spectrometry data.

Peptide	HPLC Retention Time (min:sec)	Mass	
		Calculated	Observed
N_3S-Probestin	13:00	817.5	818.4
ReO-N_3S-Probestin	14:14 (minor) 14:35	1017.4	1018.3
^{99m}TcO-N_3S-Probestin	14:54	-	-
N_3S-PEG_2-Probestin	11:50	920.5	921.5
ReO-N_3S-PEG_2-Probestin	13:37	1120.4	1121.4
^{99m}TcO-N_3S-PEG_2-Probestin	13:39	-	-

TABLE 2

Biodistribution of ^{99m}TcO-N_3S-PEG_2-Probestin in HT-1080 tumor bearing nude mice at 1 hr p.i. Values are expressed as the mean ± SD; N = 4.

Tissue	%ID/g of tissue	%ID/organ
Blood	0.60 ± 0.33	0.74 ± 0.41
Heart	1.18 ± 0.22	0.12 ± 0.02
Lung	0.91 ± 0.53	0.15 ± 0.02
Liver	12.0 ± 0.8	12.6 ± 1.1
Spleen	2.40 ± 0.45	0.28 ± 0.07
Stomach	1.28 ± 0.59	0.54 ± 0.19
Intestine	4.78 ± 0.33	10.8 ± 1.4
Kidney	48.0 ± 3.4	15.7 ± 2.2
Muscle	0.54 ± 0.25	4.69 ± 2.14
Tumor	2.88 ± 0.64	3.63 ± 2.29
Tumor/Blood	4.8	-
Tumor/Muscle	5.3	-